On the effects of ageing and annealing on the apatite and fission-track etch rates

Raymond Jonckheere[1*], Florian Trilsch[1], Jie Liu[2], Pengfei Zhai[2], Thorsten Nagel[1]

[1]Endogene Geologie, Technische Universität Bergakademie Freiberg, Deutschland

[2]Institute of Modern Physics, Chinese Academy of Sciences, Lanzhou, Gansu 730000, China

Abstract

Fission tracks in apatite must be etched to be counted and measured with an optical microscope. Track etching is described with the aid of two velocities: the track etch rate v_T and the apatite etch rate v_R. The efficiencies of track counts, the selection of confined tracks, and the distinctive shapes of etched tracks depend on the values of v_T and v_R; v_R is also an indicator of the apatite composition and annealing kinetics. Despite their importance, measurements of v_T and v_R have long been lacking. We report measurements of v_T and v_R and investigate the factors controlling them. Our results support a constant core model, i.e., a constant v_T over most of the track length. The host-confined-track intersections, ***c***-axis angles, and track-etch rates have near-identical distributions across all experiments. Neither lab annealing of induced tracks nor geological ageing of fossil tracks have a significant effect on v_T. Overall, for a standard one-step etch protocol, the lengths of fission tracks exhibit a weak positive correlation with their track etch rates and effective etch times. The effect is however too small to be significant for geological applications. When using a step-etch protocol, the etchant advances at a finite rate along tracks etched during preceding steps. This broadens the effective-etch-time and track-length distributions, while the total immersion time overestimates the aggregate effect of the procedure. In contrast to v_T, v_R exhibits clear variation related to damage from self-irradiation in the case of fossil tracks and to a minor extent from neutron irradiation in case of induced tracks. Greater v_R shorten the access times to confined tracks, increasing their effective etch times. This implies a need for caution when using the track openings for assessing annealing rates.

Keywords

Apatite, fission track, etching, track etch rate, apatite etch rate

*corresponding author: raymond.jonckheere@geo.tu-freiberg.de

1. Introduction

The fission-track method is a useful tool for dating rocks and retracing their low-temperature thermal histories. It is based on counting and measuring the damage trails from uranium fission in minerals. Apatite is the most studied mineral, and the focus of this investigation. Fission tracks in apatite shorten and fade over a range of temperatures relevant to geological processes such as basin subsidence and uplift, erosional and tectonic unroofing, thrust tectonics, and hydrocarbon maturation. Apatite grains separated from a rock are mounted in resin, polished, and etched for examination with an optical microscope. Etching creates channels along the damage trails left by the fission fragments. In contrast to unetched tracks, which have nanometre diameters, etched tracks have micrometre diameters, suitable for counting and measuring. From the outset, track etching has been described in terms of two velocities: the etch rate, v_T, of the damaged lattice along the track and the bulk etch rate, v_B, of the undamaged apatite in other directions (Fleischer and Price, 1964; Hurford, 2019). Their values determine the etching and counting efficiencies of different crystal faces (Gleadow, 1981; Tagami and O'Sullivan, 2005), and the roundedness of the confined track tips (Ketcham and Tamer, 2021). These factors determine which grains are suitable for counting and dating and which tracks are suitable for measurement and time-temperature modelling.

Little is known for certain about the factors that affect the apatite and track etch rates. It is known that v_B is anisotropic (Gleadow, 1981), and also depends on the apatite composition (Burtner et al., 1994; Carlson et al., 1999). We know less about v_T, which is assumed constant (Laslett et al., 1984) or related to the track radius or damage density (Ketcham and Tamer, 2021; Li et al., 2023). Following principles of crystal growth and dissolution (Gross, 1918; Heimann, 1975; 1982), we redefined the apatite etch rate (v_R) as the displacement rate of a plane surface as a whole instead of that of each point on the surface (v_B; Jonckheere et al., 2019; 2022). We examined how v_R varies with composition (Trilsch et al. 2023; Fu et al., 2024) and with orientation, noting steep minima parallel and perpendicular to the ***c***-axis (Aslanian et al., 202 1). Here we investigate factors affecting v_R and v_T. Section 2 focuses on the variation of v_T along tracks, section 3 on the effect of annealing, and section 4 on that of ageing on v_R and v_T. The discussion is based on the cumulative frequencies of the measured quantities. Additional scatter plots and histograms are presented in the supplements.

2. Variation of v_T along tracks

2.1 Experiment

This experiment was carried out on a single crystal of the Durango apatite from Mexico (Foshag, 1929; Young et al., 1969; McConnel, 1973). Durango apatite contains 7-22 ppm U and 150-380 ppm Th (Boyce and Hodges, 2005; Enkelmann et al., 2005a) and has a fission-track age of ~31.5 Ma (Jonckheere et al., 1993; Jonckheere, 2003, Enkelmann et al., 2005b; Jonckheere et al., 2015; 2024b). We mounted a prism section of Durango apatite in resin, ground, and polished it with 6-µm, 3-µm, and 1-µm diamond suspensions and a 0.04-µm silica suspension to expose a flat internal surface. We covered the mount with a 180-µm Al degrader foil and 12-µm PET film, and irradiated it perpendicular to the ***c***-axis and at ¼π dip angle with 25.0 MeV·amu^{-1} ^{86}Kr-ions at the HIRFL in Lanzhou, operated by the Institute of Modern Physics of the Chinese Academy of Sciences (Figure 1). We etched the mount in 5.5 M HNO_3 at 21 °C for 20 s + 10 s + 10 s to reveal the ion tracks (Figure 2). The sample had a sealed natural crack extending from the surface to tens of microns below it. Although no etchant could penetrate along it, the crack nevertheless constituted a break in the apatite lattice. The intersections of the Kr tracks with the crack are therefore convex, like their intersections with the surface, causing etch figures bounded by the fastest-etching faces to develop (Aslanian et al., 2021; Jonckheere et al., 2022). This produces uniform etch pits at the apatite surface, one side of which, with length *Dpar*, is parallel to the ***c***-axis (Burtner et al., 1994).

The same process takes place on either side of the crack, giving rise to diamond-shaped etch figures, whose size decreases with increasing distance along the track from its surface intersection (Figure 2a).

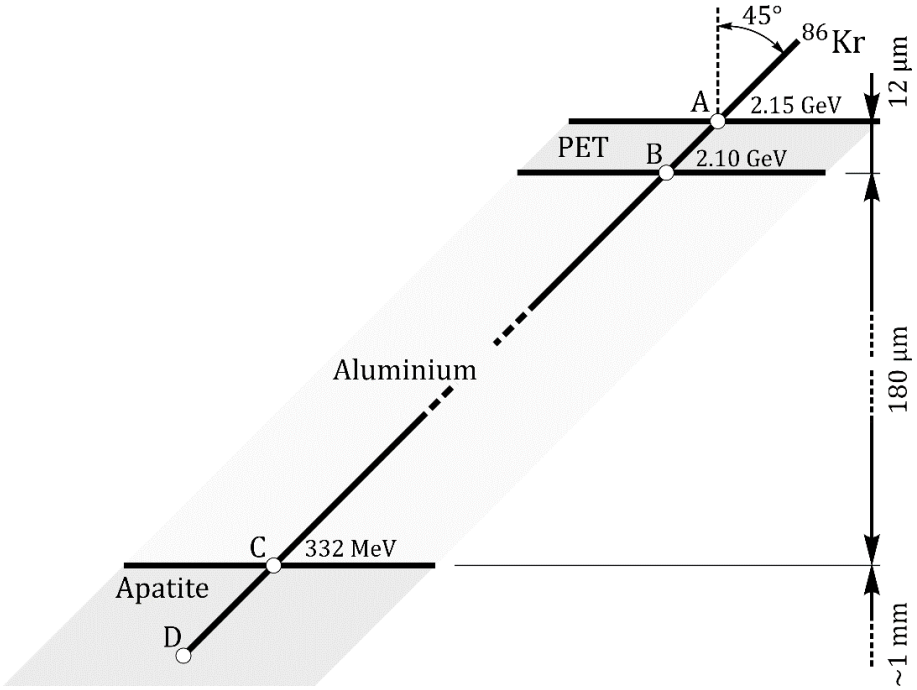

Figure 1. Kr irradiation: a prism section of an unannealed single Durango apatite is covered with a 180 µm Al degrader and a 12 µm PET film, and irradiated perpendicular to the apatite ***c***-axis and at ¼π dip angle with 25.0 MeV·amu^{-1} ^{86}Kr. The samples were etched in 5.5 M HNO_3 at 21 °C for 20 s + 10 s + 10 s to reveal the tracks.

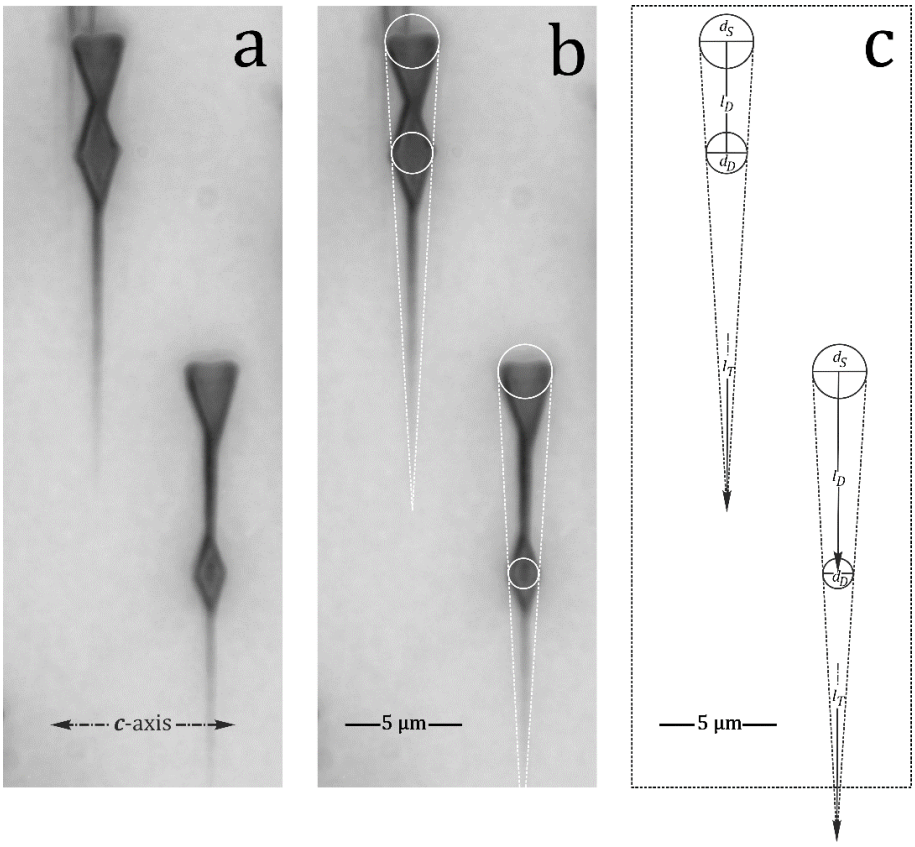

Figure 2. Compressed image stack of Kr-tracks perpendicular to the ***c***-axis, intersecting an apatite prism face (**a**, **b**); their measurements are shown in (**c**): d_S and d_D are the diameters of circles tangent to the outside edges of the triangle- and diamond-shaped etch figures at their intersections with the surface and with a crack; l_D is the distance between their centres, and l_T the measured distance to the end of the etched section.

From the diameters (d_S, d_D) of circles tangent to their outside edges (Figures 2b,c), and the immersion time (t_I) we calculate the effective etch time $t_E = (d_D / d_S)\, t_I$, and access time, $t_A = t_I - t_E$, of each diamond shape, i.e., the time that the etchant needs to advance from the surface to the crack. After correcting for dip, the etched distance to the crack is $l = l_D / \cos(¼\pi)$ and the total etched length is $l_M = l_T / \cos(¼\pi)$.

2.2 Results

Table 1 reports the measurements for the 20 s, 30 s, and 40 s cumulative immersion times. Figure 3a plots d_D against l; Figure 3b shows histograms of the calculated lengths l_M. The solid lines in Figure 3a are geometric mean regression lines anchored at the mean values of d_S. These means have negligible error compared with the individual d_D-values, because d_S (*Dpar*) exhibits almost no variation and was measured for each track and immersion time. Table 1 lists the slopes (s) of the regression lines, along with their d-axis and l-axis intercepts, and the calculated track etch rates: $v_T = -d_S / (s\, t_I)$.

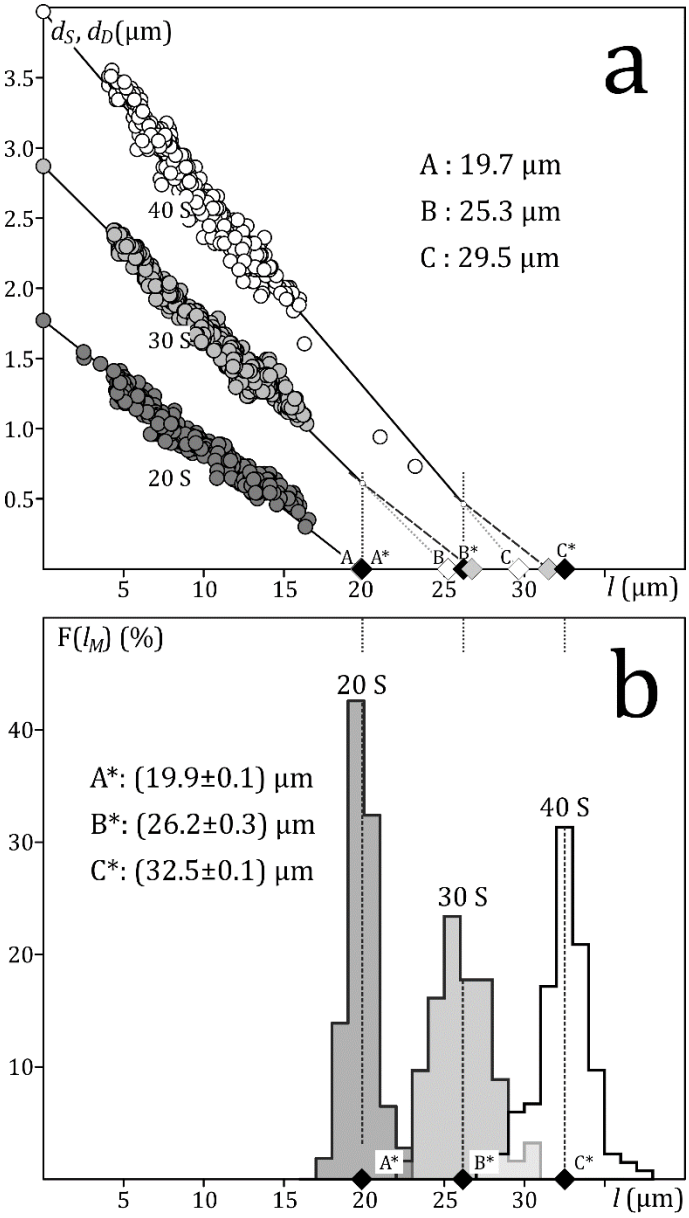

Figure 3. Results of the Kr-track length and size measurements. **(a)** Diamond sizes (d_D) plotted against distance along the track ($l = l_D/\cos(¼\pi)$) for 20 s (dark), 30 s (light), and 40 s (white) immersion. The intercepts (d_S) at $l = 0$ are the average *Dpar*. The solid lines are geometric mean regression lines anchored at d_S. The white diamonds at A (20 s; hidden), B (30 s), and C (40 s) are the intersections (l_I) of the regression lines with the l-axis. The black diamonds at A* (20 s), B* (30 s), and C* (40 s) are the corresponding measured lengths (l_M; Figure 3b). The dashed lines and grey diamonds (l_E) are extrapolations of the 30 s, and 40 s values at A* and B*, assuming that the unetched sections beyond A* and B* etch at the rate calculated from the 20-s data **(b)** Histograms of the measured track lengths ($l_M = l_T/\cos(¼\pi)$) for 20 s, (20+ 10) s, and (30 + 10) s etching in 5.5 M HNO_3 at 21 °C. A*, B*, and C* are the mean lengths plotted in (a) (black symbols).

t_I	n_T	s_R	v_T	d_S	$\Delta d_S/\Delta t_I$	l_I	l_M	l_E	t_M
20	467	-0.090	59.6	1.77(1)	0.089(5)	19.7	19.9(1)	19.8	20.1
30	514	-0.113	276	2.87(1)	0.110(4)	25.3	26.2(3)	26.7	32.1
40	363	-0.135	324	3.97(1)	0.110(3)	29.5	32.5(1)	31.1	40.8

Table 1. Measurements of Kr-tracks in a Durango apatite prism face etched 20, 30, and 40 s in 5.5 M HNO_3 at 21 °C. t_I (s): immersion time; n_T: number of tracks; s_R: slopes of geometric mean regression lines, anchored at d_S, fitted to d_D vs. l (Figure 3a); v_T (μm·min^{-1}): rate of etchant advance calculated from s_R; d_S (μm) and l_I (μm): d- and l-axis intercepts of the regression lines; l_M (μm): mean measured lengths (Figure 3b) l_E (μm): calculated mean etched length, assuming a constant track etch rate v_T (Figure 3a); t_M (s): immersion times corresponding to the measured mean lengths and calculated etch rates.

2.3 Discussion

The v_T-value for the initial 20-s immersion ($v_T \approx 60$ μm·min^{-1}) is the actual track etch rate. The value is comparable with that for induced fission tracks at high angles to the ***c***-axis in a prism section of Durango apatite (Figure 5c in Jonckheere et al., 2024a). The values for 30 s and 40 s immersion measure the fast but finite rate of etchant advance along pre-etched tracks. The sum of the immersion times of a step-etch experiment therefore overestimates the effective cumulative etch time. For the Kr tracks, this amounts to ≳4 s for the 10-s step following the initial 20-s immersion; i.e., the time required to travel the length (≈20 μm) of the pre-etched track section at $v_T \approx 275$ μm·min^{-1} (20 μm /4.6 μm·s^{-1}≈ 4.3 s). Step-etching thus broadens the effective-etch-time distributions of ion and fission tracks (Figure 8 of Trilsch et al., 2023; Figure 6a of Jonckheere et al., 2024a).

The difference between the measured mean length and the l-axis intercept of the regression line for the first 20 s step (l_M - l_I) is negligible but increases at each subsequent step (Table 1; Figure 3). This is because the high etch rates during later steps relate to the track sections etched during the preceding step but not to the unetched sections beyond them, which etch at the normal rate v_T. We corrected the expected lengths (l_E), based on the measured lengths and etch rates in Table 1 (caption of Figure 3). The accord between the revised and measured lengths (l_M - l_E) and between the revised and actual immersion times (t_M - t_I) is reasonable, considering the uncertainties. In particular the high etch rates of the pre-etched sections affect the calculations because they are obtained from the small differences between the slopes of the regression lines fitted to the 20-, 30-, and 40-s data. The calculation assumes a constant v_T over the entire etched track length up to 40 s (constant core; Tamer and Ketcham, 2020a). The results in Figure 3a and Table 1 support this assumption.

A constant v_T is consistent with the fact that fission tracks in apatite have straight sides, lacking curvature (Figures 4a and 4b; 'motorboat effect'; Fleischer et al., 1969; 1975; Paretzke et al., 1973; Somogyi and Szalay, 1973; Durrani and Bull, 1987; Nikezić, 2000; Nikezić and Yu, 2003; 2004). This means that v_T is unrelated to the local stopping power (Tamer and Ketcham, 2020a; Ketcham and Tamer, 2021), or to the radius of the latent track (Li et al., 2012; 2014). The most compelling indication is that etched confined tracks show no constriction, interruption or other modification in their midsections, even though the effective fission fragment charges, and thus stopping power and track radius are assumed to be near zero at the locus of the fissioned nucleus (Li et al., 2023). We have earlier reported that the average fission track etch rate varies with *Dpar* (Fu et al., 2024) and with the track orientation, with minima parallel and perpendicular to the ***c***-axis, analogous to the apatite etch rate v_R (Jonckheere et al., 2024a). This suggests that v_T is more

related to the chemical characteristics of the track detector than to the properties of the fission fragments.

The fact that the mean etch pit size increases less in relation to the immersion time during the initial 20-s immersion, than during the subsequent 10-s immersions (Table 1; $\Delta d_S/\Delta t_I$) is due to an etch induction time related to polishing damage (Jonckheere and Van den haute, 1996, their Figure 19).

3. Effect of annealing on v_T and v_R

3.1 Experiment

To investigate the effects of partial annealing on v_T and v_R, we carried out track measurements on four prism sections of Durango apatite that had been pre-annealed, neutron-irradiated and, all but one, re-annealed to create induced-track populations with mean lengths of ~16 µm (sample 21-2), ~14 µm (21-4), ~12 µm (21-1), and ~10 µm (21-3). The irradiation and annealing conditions are given in Ketcham et al. (2015). The track densities measured in transmitted and reflected light are reported in Aslanian et al. (2022). The samples were mounted in resin, polished with 6-µm, 3-µm, and 1-µm diamond and 0.04-µm silica suspensions, and etched for 20 s in 5.5 M HNO_3 at 21 °C (Carlson et al., 1999). The confined tracks were imaged and measured as in Jonckheere (2023). The measurements included the track lengths, orientations, widths, cone-angles, the positions of the host track intersections (i_P), and *Dpar*. We calculated the effective etch times and the apatite and track etch rates using the equations of Aslanian et al. (2021) and Fu et al. (2024).

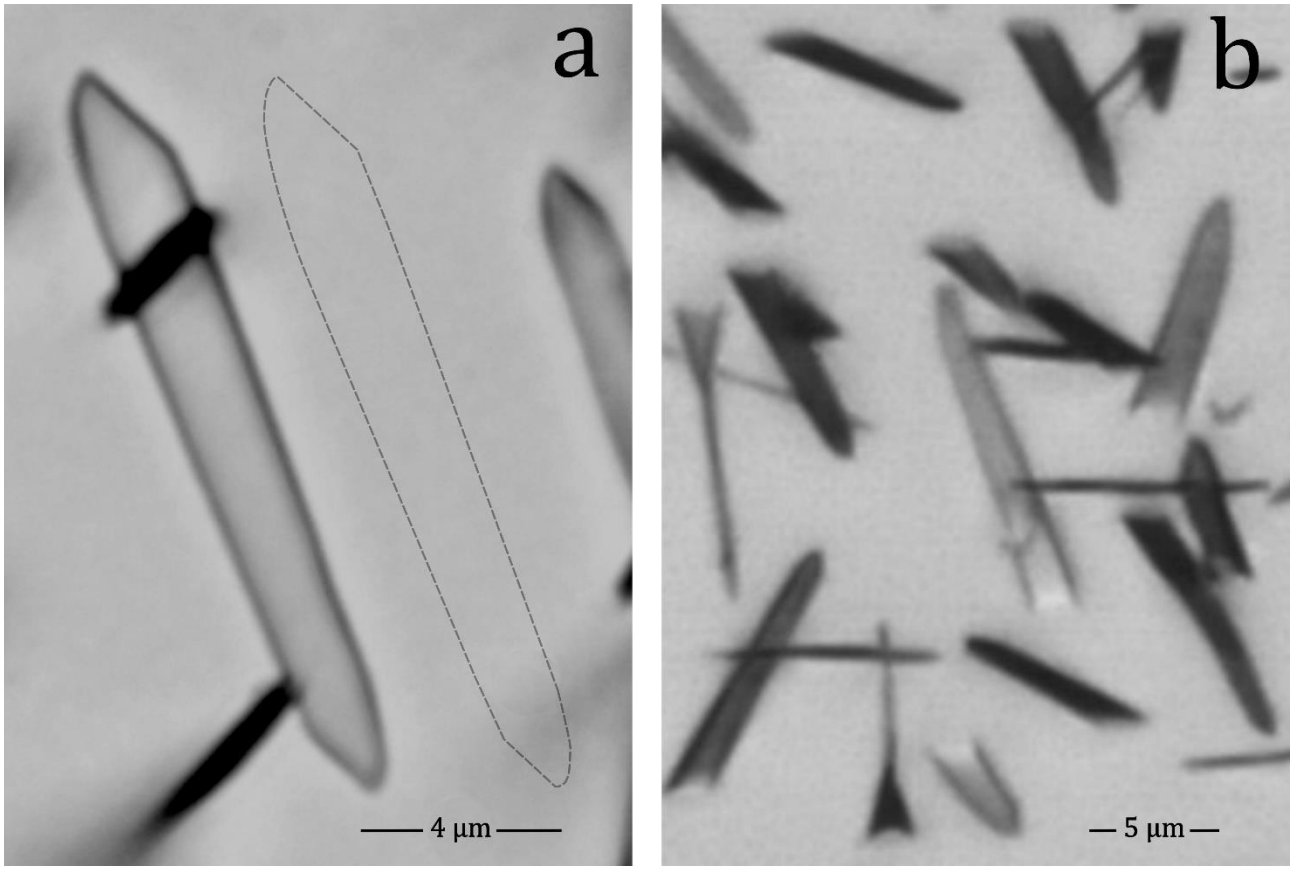

Figure 4. Etched fission tracks in an apatite prism face showing the characteristic straight-sided outline, consistent with constant v_T: **(a)** horizontal confined track; **(b)** compressed image stack of surface tracks (etched 20 s in 5.5 M HNO_3 at 21°C).

3.2 Results

Figures 5 and 6 show the cumulative distributions of the measured track properties for different annealing stages; Table 2 lists the main statistics. It is worth noting that the angular (azimuth) distribution remains unchanged after partial annealing (Figure 5d). This is similar to the results of Ketcham (2003), except that our data cover mean lengths from 15.9 µm to 10.1 µm, before ***c***-axis projection (Supplement Figure 1d). The intersection-point distribution (from host track to the nearest tip) is also unaffected by annealing (Figure 6a). In each sample, the number of intersections decreases from the centre towards the track tips (Supplement Figure S04) but there is no evidence that, in relative terms, short tracks are differently affected than long tracks. The general decrease from the centre towards the tips could be attributed to the fact that a confined tracks intersected near its tip cannot be measured if it is obscured by the host track. In that case one would expect that, in relative terms, the effect is greater for short tracks than for long tracks, which is not so. One might conjecture that there is a countervailing bias of some sort, perhaps related to a change of the track etch rate due to annealing. We rule this out because our evidence shows that there is no v_T-change, and because it is improbable that two unquantifiable biases exactly cancel (Figure 6a). We therefore prefer to consider a factor that is constant across the annealing stages and mean lengths. There is e.g., the fact that it takes twice as long to etch a track intersected at one tip than a track intersected in its centre to the point that both tips are etched so that the track is accepted for measurement. Tracks intersected between their tips and centre will require an intermediate etching time. This could account for the gradual decrease of the intersection point frequencies starting from the track centre towards the track tips (supplement Figure S04). This supports a constant-core v_T-model, as a linear model entails that the time required to reach the furthest tip depends sensitively on the intersection point. These observations are counter to expectation based on length bias and anisotropic annealing (Galbraith et al., 1990; Donelick et al., 1999; Galbraith, 2002; Ketcham, 2003). It has been established that track selection is not just a matter of geometrical biases, but that etching and observer biases must also be taken into consideration. According to Aslanian et al. (2021) and Jonckheere (2023), the selection of a confined track depends on whether it exceeds a threshold width, which is not affected by annealing.

3.3 Discussion

The cumulative v_T-distributions are the same after 10-h annealing at 240 °C (21-4), 288 °C (21-1), and 310 °C (21-3; Figure 6b) as that of unannealed induced tracks (21-2), despite experiencing mean length reductions of ~2, ~4, and ~6 µm. This contradicts the finding that partial annealing of induced tracks at 235 °C to 280 °C causes up to a doubling of v_T (Ketcham and Tamer, 2021). Taken together with the fact that v_T exhibits no variation along the tracks (section 2) and is unaffected by lab-annealing, the observations that v_T correlates with *Dpar* (Fu et al., 2024) and varies with the angle to the apatite ***c***-axis (Jonckheere et al., 2024a) underscore the fact that v_T is more a function of the detector properties than of the damage densities along the fission fragment trajectories.

The median effective etch time of the unannealed tracks (21-2) is 2 s longer than that of the most annealed (21-3; Figure 6c). Both intermediate samples lie between the extremes, albeit in reverse order. Given that their track and apatite etch rates are almost the same, one might expect that t_E correlates with the reciprocal track densities. That of 21-3 is ~⅔ of 21-2 (Aslanian et al., 2022); the average separation between a host track and a potential confined track in 21-3 is thus greater than in 21-2. However, this must not be the case for the measured tracks, selected on the basis of their widths. For an average v_T of ~2 µm·s^{-1} (Table 2: ~120 µm·min^{-1}), a ~2-s t_E-difference corresponds to a ~4-µm length difference in the etchant trajectories from the host track intersections to the confined-track tips. If the host track intersects a confined track in the middle, we have 2 × 4 µm = 8 µm; if it intersects it at the tip and etches in one direction, we have 4 µm. The average is ½ (4 µm + 8 µm) = 6 µm. This is correlates well with the ~6 µm mean-length difference between 21-2 and 21-3.

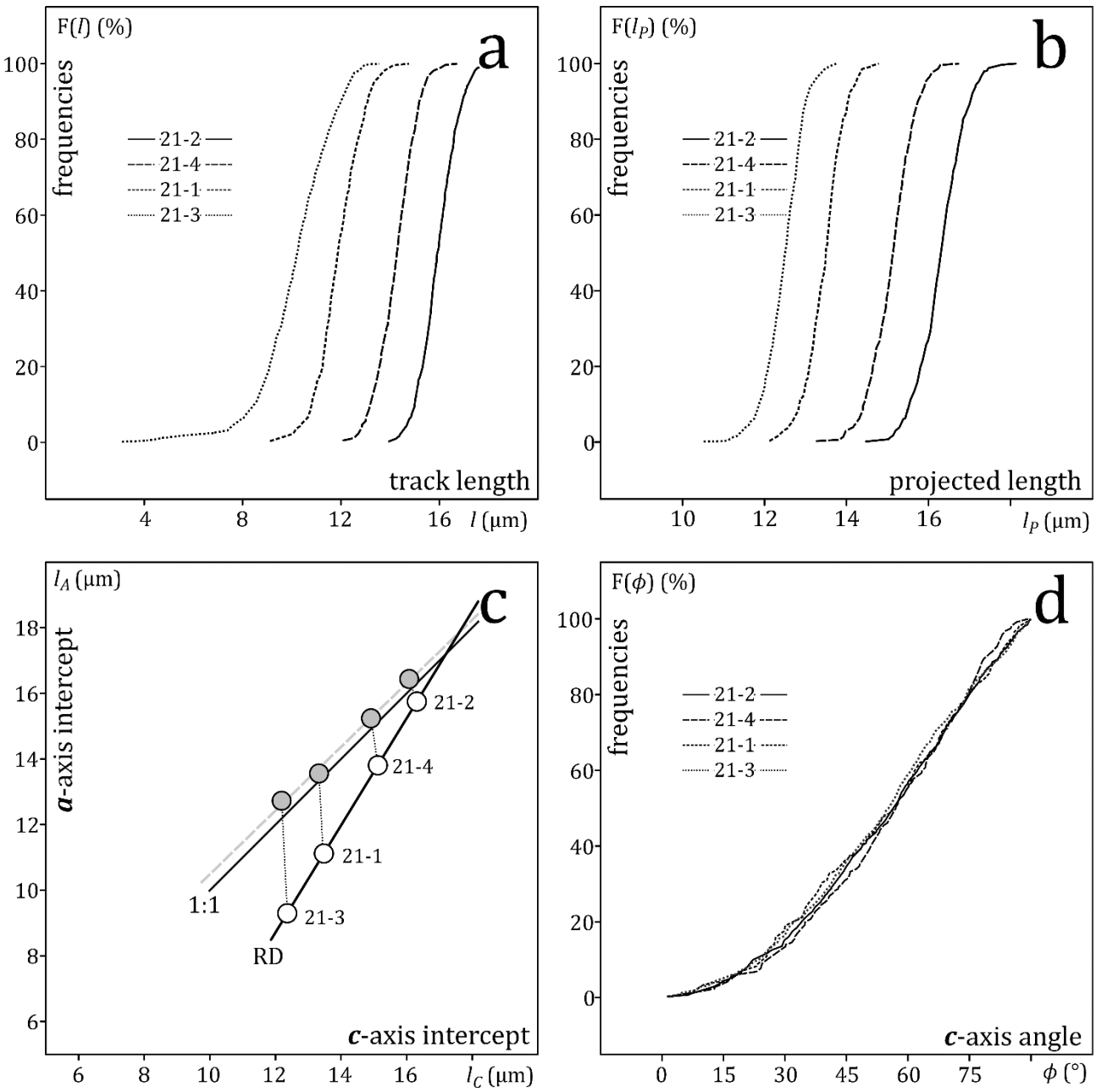

Figure 5. (a) Cumulative frequencies of the lengths (l) of horizontal induced confined tracks in prism faces of four Durango apatites with increasing degrees of annealing, distributed as part of an inter-lab experiment (Ketcham et al., 2015; 21-2: unannealed; 21-4: annealed 10 h at 240 °C; 21-1: annealed 10 h at 288 °C; 21-3: annealed 10 h at 310 °C). **(b)** Cumulative frequencies of the ***c***-axis projected lengths (l_P). **(c)** The ***a***-axis (l_A) vs. ***c***-axis intercepts (l_C) of ellipses fitted to the length (l) vs. ***c***-axis angle (ϕ) data (white; RD: $l_A = 1.632\ l_C - 10.879$; empirical relationship of Donelick et al., 1999), and of regression lines fitted to the ***c***-axis projected length (l_P) vs. ***c***-axis angle (ϕ) (grey; 1:1: isotropic line: $l_A = l_C$); **(d)** cumulative frequencies of the ***c***-axis angles.

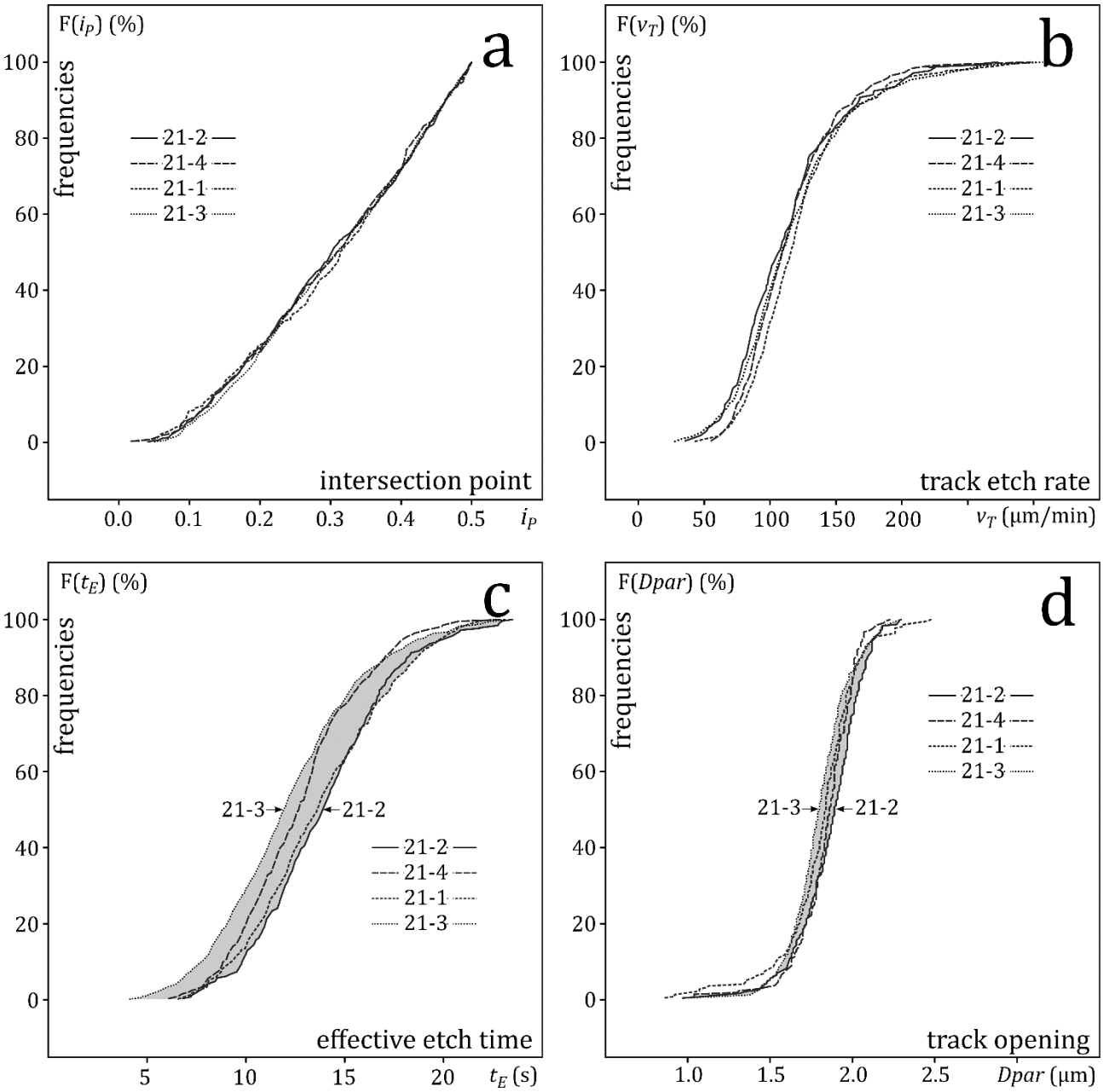

Figure 6. (a) Cumulative frequencies of the intersections (i_P) between host-track and confined track, measured from the intersection to the closest track tip and normalised to the confined track length. **(b)** Cumulative frequencies of the calculated track etch rates (v_T). **(c)** Cumulative frequencies of the calculated effective etch times (t_E). **(d)** cumulative frequencies of the size of the track surface intersections parallel to the ***c***-axis (*Dpar*).

LSTD	N_C	l_M	s_M	l_{50}	l_P	s_P	l_{P50}	l_C	l_A	l_{PC}	l_{PA}
21-2	572	15.9(1)	0.75	15.9	16.3(1)	0.56	16.3	16.3(1)	15.7(1)	16.1(1)	16.4(1)
21-4	370	14.2(1)	0.77	14.3	15.1(1)	0.52	15.1	15.1(1)	13.8(1)	14.9(1)	15.2(1)
21-1	332	11.9(1)	0.90	11.8	13.5(1)	0.46	13.5	13.5(1)	11.1(1)	13.3(1)	13.6(1)
21-3	801	10.1(1)	1.49	10.3	12.5(1)	0.47	12.5	12.4(1)	9.3(1)	12.2(1)	12.7(1)

LSTD	N_D	*Dpar*	s_D	D_{50}	N_E	t_E	s_E	t_{50}	N_{VT}	v_T	s_T	v_{50}
21-2	219	1.81(2)	0.25	1.89	568	13.3(1)	3.4	12.4	607	127(2)	44	114
21-4	231	1.87(2)	0.20	1.86	368	12.2(2)	3.0	11.4	426	123(2)	41	111
21-1	239	1.80(1)	0.19	1.84	329	13.2(2)	3.2	12.4	328	123(3)	47	107
21-3	212	1.84(1)	0.18	1.80	799	11.5(1)	3.5	10.4	697	123(2)	48	105

Table 2. Measurements of confined tracks in unannealed and part-annealed prism faces of Durango apatite etched for 20s in 5.5 M HNO_3 at 21 °C. LSTD: length standard; N_C: number of confined track lengths; l_M: mean length (µm); s_M: standard deviation (µm); l_{50}: median; l_P: mean of ***c***-axis-projected lengths (µm); s_P: standard deviation of the ***c***-axis-projected lengths (µm); l_{P50}: median projected length;(l_C, l_A): ***c***-axis and ***a***-axis intercepts of ellipses fitted to length vs. orientation data (µm); (l_{PC}, l_{PA}): ***c***-axis and ***a***-axis intercepts of regression lines fitted to projected-length vs. orientation data (µm). N_D: Number of *Dpar*-measurements; *Dpar*: mean *Dpar* (µm); s_D: standard deviation (µm); D_{50}: median (µm); N_E: number of effective-etch-time measurements; t_E: mean effective etch time (s); s_E: standard deviation (s); t_{50}: median effective etch time (s); N_{VT}: number of track etch rate measurements; v_T: mean track etch rate (µm·min^{-1}); s_T: standard deviation (µm·min^{-1}); v_{50}: median track etch rate (µm·min^{-1}). Numbers in brackets are standard errors on the last digit, which are ≪1 µm due to the law of large numbers, i.e., the error of the mean decreases with the square root of the number of measurements. Moreover, the cited errors reflect the precision of the measurements, which is not limited by the Abbé rule relating to their resolution (Bobroff, 1986; Copeland et al., 2018).

All samples have narrow *Dpar*-distributions with medians (D_{50}) decreasing from 1.89 µm for the unannealed apatite (21-2) to 1.80 µm for the most annealed (21-3). The difference is small but reflects a systematic shift of the *Dpar*-distribution to lower values with increasing annealing (Figure 6d). Because *Dpar* is proportional to the apatite etch rate, it suggests a thermal relaxation of irradiation-induced strain from recoils following (n,γ)-reactions or uranium fission and track formation (Rivera et al., 2011; Dufour and Toulemonde, 2016; Schauries, 2018; Rymzhanov et al., 2019). Assuming Arrhenius kinetics, the D_{50}-ratio (1.80(2)/1.89(2) = 0.953(15)) of the most annealed and unannealed samples represents an activation energy increase for apatite etching of 118(27) J·mol^{-1}, or 1.22(28) meV per atom. If an individual point defect stores ~1 eV, the lowering of the apatite etch-rate results from annealing one in a thousand (F_D = 1.22×10^{-3}) defects created by irradiation.

Assuming Arrhenius kinetics, the rate factor (k_D) and activation energy (E_D) for defect annealing are given by:

$$k_D = \frac{ln(1-F_D)}{t_A} = 3.39(78) \times 10^{-8} s^{-1} \quad (1)$$

wherein t_A = 36000 s is the annealing time (10 h). For a pre-exponential factor $k_0 = 10^{13}$ s^{-1}, this gives:

$$E_D = RT_A ln\left(\frac{k_0}{k_D}\right) = 228(1)\ \mathrm{kJ \cdot mol^{-1}} \quad (2)$$

wherein R = 8.314 J·K^{-1}·mol^{-1} is the gas constant, and T_A = 310 °C the annealing temperature of 21-3. For comparison, we calculated corresponding nominal rate factors (k_F) and activation energies (E_F) for fission-track annealing using the fractional length reduction, $F_F = 1 - l/l_0$, to measure progress. The calculation shows that E_F increases from 181(1) kJ·mol^{-1} at 240 °C to 202(1)

kJ·mol^{-1} at 310 °C (Table 3). These are indicative average values, conditional on the assumed Arrhenius kinetics and the pre-exponential constant (k_0). Without, therefore, attaching undue physical meaning to the numerical results, the calculation bears out that fission-track annealing and the lowering of the apatite etch rate due to partial elimination of point defects both occur under the annealing conditions to which the samples were exposed. On the whole, point defects begin to anneal at time-temperature conditions at which fission-track annealing is already well advanced.

LSTD	T_{AN} (°C)	t_{AN} (h)	T_{AN} (K)	t_{AN} (s)	F_F	k_F (10^{-6}·s^{-1})	E_F (kJ·mol^{-1})
21-4	240	10	513	36000	0.101(1)	2.81(03)	181(1)
21-1	288	10	561	36000	0.258(3)	7.17(08)	195(1)
21-3	310	10	583	36000	0.352(4)	9.78(11)	202(1)

Table 3. Activation energies for fission-track annealing. T_{AN}: annealing temperature in °C and in K; t_{AN}: annealing time in hours and in seconds; F_F: fractional annealing $F_F = 1 - l/l_0$; k_F: rate factor; E_F: activation energy. Errors are 1σ.

For a constant-core model and high average track etch rate ($v_T \approx 120$ µm·min^{-1}; Table 2), the exact value of v_T and the precise point from where a confined track begins to etch are of little consequence. For the same reason, the effect of multiple host track intersections, even occurring at the same time and far apart, is minimal. This is not so for a linear v_T-profile with a central maximum (~1.7 µm·s^{-1}; unannealed induced tracks) decreasing to v_R towards the track tips (Ketcham and Tamer, 2021). In that case, short tracks intersected towards one end are more likely than longer tracks to be etched at the opposite end to a point that satisfies an operator's selection criteria. This would produce a correlation between the track length and the position of the host track intersection (Figure 8 of Jonckheere, 2023). The correlation would decrease depending on the extent of length reduction and the increase of the track etch rate following partial annealing (Ketcham and Tamer, 2021).

It is reasonable to suppose that the lengths of individual confined tracks depend to some extent on their host track intersections (i_P), track etch rates (v_T), and effective etch times (t_E). To exclude spurious correlations due to length anisotropy, we plotted the ***c***-axis-projected lengths (l_P) against i_P, v_T and t_E. Regression lines to the l_P-vs.-i_P plots of 21-2 and 21-4 have small positive slopes whereas those to the l_P-vs.-i_P plots of 21-1 and 21-3 have small negative slopes, indicating the absence of a significant correlation (Figure S07). Regression lines to the l_P-vs.-v_T plots of all the samples have small positive slopes (Figure S08). Because of the large v_T-range (50-250 µm·min^{-1}; Figure S05), this can add on average 0.1-0.3 µm to the lengths of fast-etching tracks compared to those of slow-etching tracks. Regression lines to three out of four l_P-vs.-t_E plots (except 21-4; Figure S09) have weak positive slopes, which, nevertheless, add on average 0.1-0.3 µm to the lengths of well-etched tracks ($t_E \approx 20$ s) compared to those of underetched tracks ($t_E \approx 5$ s). Because the independent variables are not free from measurement error, least squares regression underestimates the true slopes and overestimates the intercepts of the regression lines due to attenuation bias. If half of the measured variation of v_T and t_E is true variation and the remainder due to measurement error, the true slopes would be twice as high, and the l_P-ranges, $\Delta(v_T)$ and $\Delta(t_E)$, should be doubled. We nevertheless conclude that, for practical purposes, within a sample of confined tracks selected for measurement, the intersection points, the track etch rates and the effective etch times have little effect on the length distribution (20 s; 5.5 M HNO_3; 21 °C). This does not mean, however, that they have no effect on the sampling itself, i.e., on the distinction between tracks selected for measurement and those that are not. E.g., the effective etch time influences the widths of confined tracks, and so their qualification for measurement.

4. Effect of ageing on v_T and v_R

4.1 Experiment

We studied the FC1 and AS3 apatites from the Duluth intrusive complex in Minnesota to investigate the effects of geological ageing. FC1 and AS3 are reference materials and proposed age standards with fission-track ages of 820(27)-882(44) Ma (FC1), and 924(36)-989(31) Ma (AS3; Iwano et al., 2019; Cogné and Gallagher, 2021; Härtel et al., 2022; 2023; Jonckheere et al., 2024b). Their interest lies in the fact that they are old and have long low-temperature thermal histories, and so accumulated extensive radiation damage, the most important factor responsible for ageing. Based on the data of Härtel et al. (2023), the total accumulated alpha dose for FC1 is ~7×10^{16} a·g^{-1} (0.8-1.0 dpa), although it is not known what fraction of the damage survived till the present. We are not aware of such data for AS3.

We annealed an aliquot of FC1 and AS3 for 24 h at 450 °C, and irradiated it with thermal neutrons in channel Y4 of the BR1 reactor in Mol, Belgium. We mounted irradiated and untreated fractions of each sample in resin, and ground, polished and etched them using the techniques described in section 3.1. As there also, we measured the track lengths, orientations, widths, cone-angles, and *Dpar*, but not the host track intersections, and calculated the effective etch times and the apatite and track etch rates.

4.2 Results

Consistent with their similar *Dpar*-values, the induced-track length distributions of FC1 and AS3 are almost identical. The fossil tracks in both samples underwent >20% shortening; both fossil-track length distributions are also similar, although those in FC1 are somewhat shorter. We interpret this difference as significant; ***c***-axis projection highlights the greater fraction of short tracks (Table 4; Figure 7a,b). The semi-axes of ellipses fitted to the induced-track data are close to the trend for unannealed apatites (Donelick et al., 1999); those fitted to the fossil-track data reveal them to be somewhat less anisotropic than induced tracks of the same mean length (Figure 7c). This could be due to different length bias affecting high- and low-angle tracks, different angular distributions, which control the relative weights of the constituent populations, or under-etching (Jonckheere, 2023; Jonckheere et al., 2024a). However, the angular distributions of the fossil, as well as induced, tracks are almost identical (Figure 7d) and the effective etch times of the fossil tracks are 1-2 s longer than those of the induced (Table 4; Figure 8b). This argues against experimental factors, leaving length-bias as the likeliest cause, barring unknown differences between fossil and induced tracks.

DULU	N_C	l_M	s_M	l_{50}	l_P	s_P	l_{P50}	l_C	l_A	l_{PC}	l_{PA}
FC1-I	536	15.9(1)	0.83	15.9	16.3(1)	0.60	16.3	16.1(1)	15.8(1)	16.1(1)	16.4(1)
FC1-S	527	12.4(1)	1.49	12.5	13.8(1)	1.00	13.9	13.2(2)	12.0(1)	13.3(1)	14.2(1)
AS3-I	346	15.8(1)	0.86	15.8	16.2(1)	0.63	16.3	16.1(1)	15.6(1)	16.1(1)	16.3(1)
AS3-S	309	12.6(1)	1.36	12.7	14.0(1)	0.88	14.0	13.6(2)	12.1(1)	13.7(1)	14.2(1)

DULU	N_D	*Dpar*	s_D	D_{50}	N_E	t_E	s_E	t_{50}	N_{VT}	v_T	s_T	v_{50}
FC1-I	406	2.06(2)	0.34	2.11	460	10.6(2)	3.8	10.6	460	105(2)	42	99
FC1-S	384	2.41(2)	0.30	2.47	513	13.1(2)	4.1	13.1	503	99(2)	39	97
AS3-I	381	1.92(1)	0.26	1.97	300	11.2(2)	3.7	10.9	300	107(2)	41	100
AS3-S	390	2.23(1)	0.28	2.27	268	12.2(3)	4.0	12.0	267	99(3)	42	93

Table 4. Measurements of fossil and induced confined tracks in FC1 and AS3 (DULU: Duluth) apatite, etched for 20s in 5.5 M HNO_3 at 21 °C. See Table 2 for symbols.

4.3 Discussion

As in the case of the annealed Durango samples, the v_T-distributions of all the Duluth samples are almost identical (Figure 8a). The ~5% difference between the means for the fossil and the induced tracks (Table 4) is too small to be considered significant at this stage. The overall agreement is striking given that the track etch rates v_T are calculated from the apatite etch rates v_R (Fu et al., 2024):

$$v_T = \frac{s_{12}}{(d_1 - d_2)} v_{RS} \quad (3),$$

wherein s_{12} is the distance between two inscribed circles, with diameters d_1 and d_2, touching opposite sides of the confined track, and v_{RS} is the apatite etch rate perpendicular to the track axis. *Dpar*-measurements indicate that the apatite etch rate differs 7 - 8% between FC1 and AS3 and 16-17% between the fossil and induced tracks (Table 4). We applied the empirical correlation between *Dpar* and v_R (Trilsch et al., 2023; Fu et al., 2024) for calculating the apatite etch rate of each sample:

$$v_{RS} = \frac{[Dpar]_S}{[Dpar]_D} v_{RD} \quad (4).$$

$[Dpar]_S$ and $[Dpar]_D$ refer to the sample and to Durango apatite, and v_{RD} is the etch rate of Durango (Aslanian et al., 2021). The agreement between the v_T-distributions of FC1 and AS3 is perhaps unsurprising. Both are from the Duluth complex anorthosite series, albeit from locations >100 km apart, and, according to their ages and track length distributions, both had similar thermal histories. The less obvious finding is that, in contrast to the substantial length reduction, ageing, or geological low-temperature annealing, appears to have had a minimal effect on the etch rates of the fossil tracks.

As in the case of the annealed Durango samples, the average effective etch-times (t_E) of FC1 and AS3 are just over half the immersion time (t_I = 20 s; Table 4). The means, medians and standard deviations for both induced-track samples are similar, those for both fossil-track samples somewhat less so, reflecting their geological histories. There is, on the other hand, a definite offset between the t_E-distributions of the fossil and induced tracks (Figure 8b,d), which is not due to v_T. The longer effective etch times of the fossil tracks are instead due to the greater v_R of the unannealed grains, which allow faster etchant access to the confined tracks. There are contributing factors: the much higher fossil than induced track densities (Jonckheere et al., 2024b) lowers the average separation between the host tracks and confined tracks; on the other hand, the shorter fossil- than induced-track lengths have an opposite effect. It is difficult to separate these factors because the stock of confined tracks is sampled using the experimenter's track selection criteria.

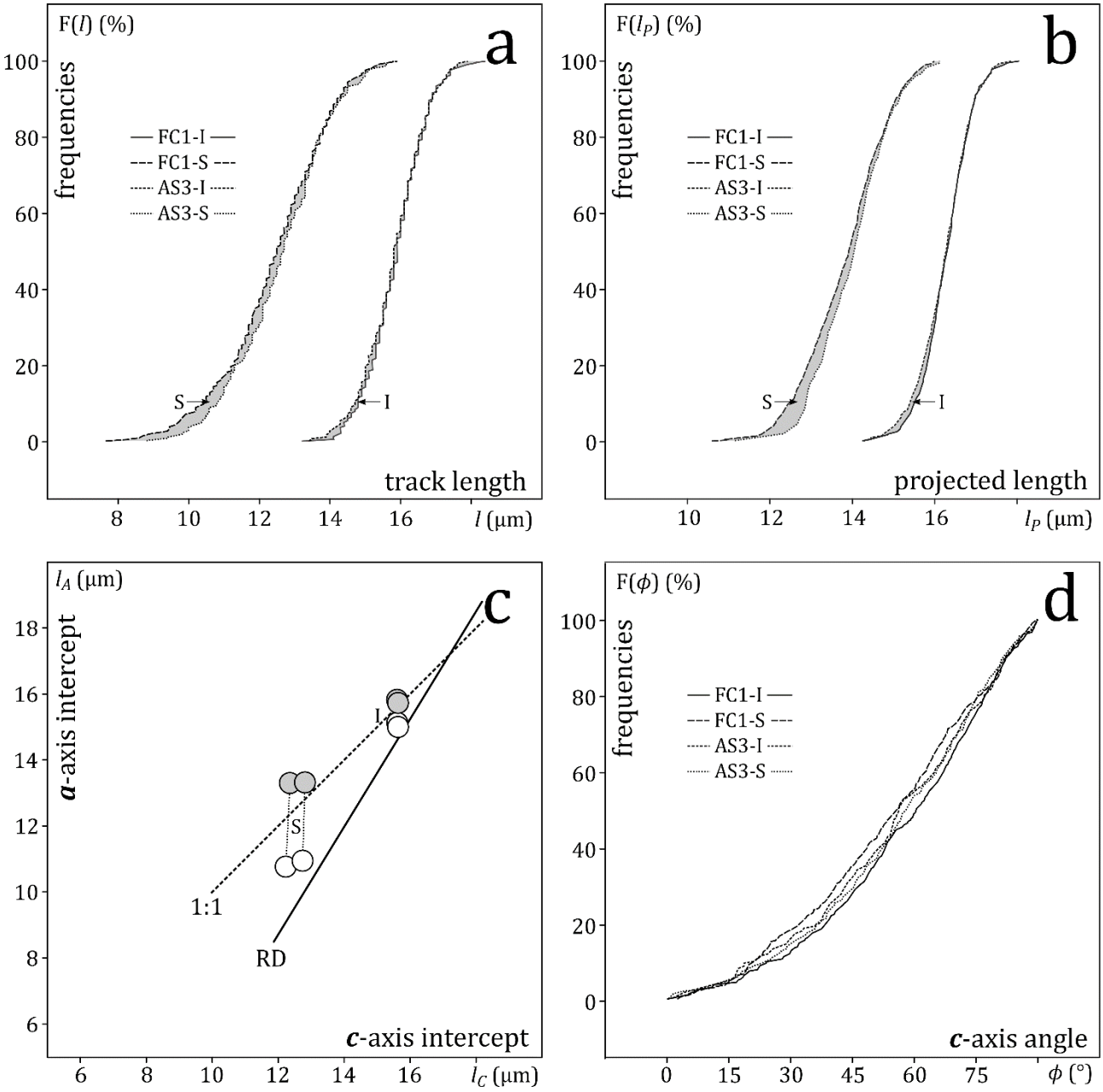

372 **Figure 7. (a)** Cumulative frequencies of the lengths of fossil (S) and induced (I) confined tracks in prism
373 faces of FC-1 and AS-3 apatites from the Duluth complex, Minnesota, USA (Iwano et al., 2019; Härtel et
374 al., 2023). **(b)** Cumulative frequencies of the ***c***-axis projected lengths of FC-1 and AS-3. **(c)** ***a***-axis vs. ***c***-
375 axis intercepts of ellipses fitted to the lengths and regression lines fitted to the ***c***-axis projected length
376 vs. ***c***-axis angle (white: induced; grey: fossil; RD and 1:1 as in Figure 5); **(d)** cumulative frequencies of
377 the ***c***-axis angles.

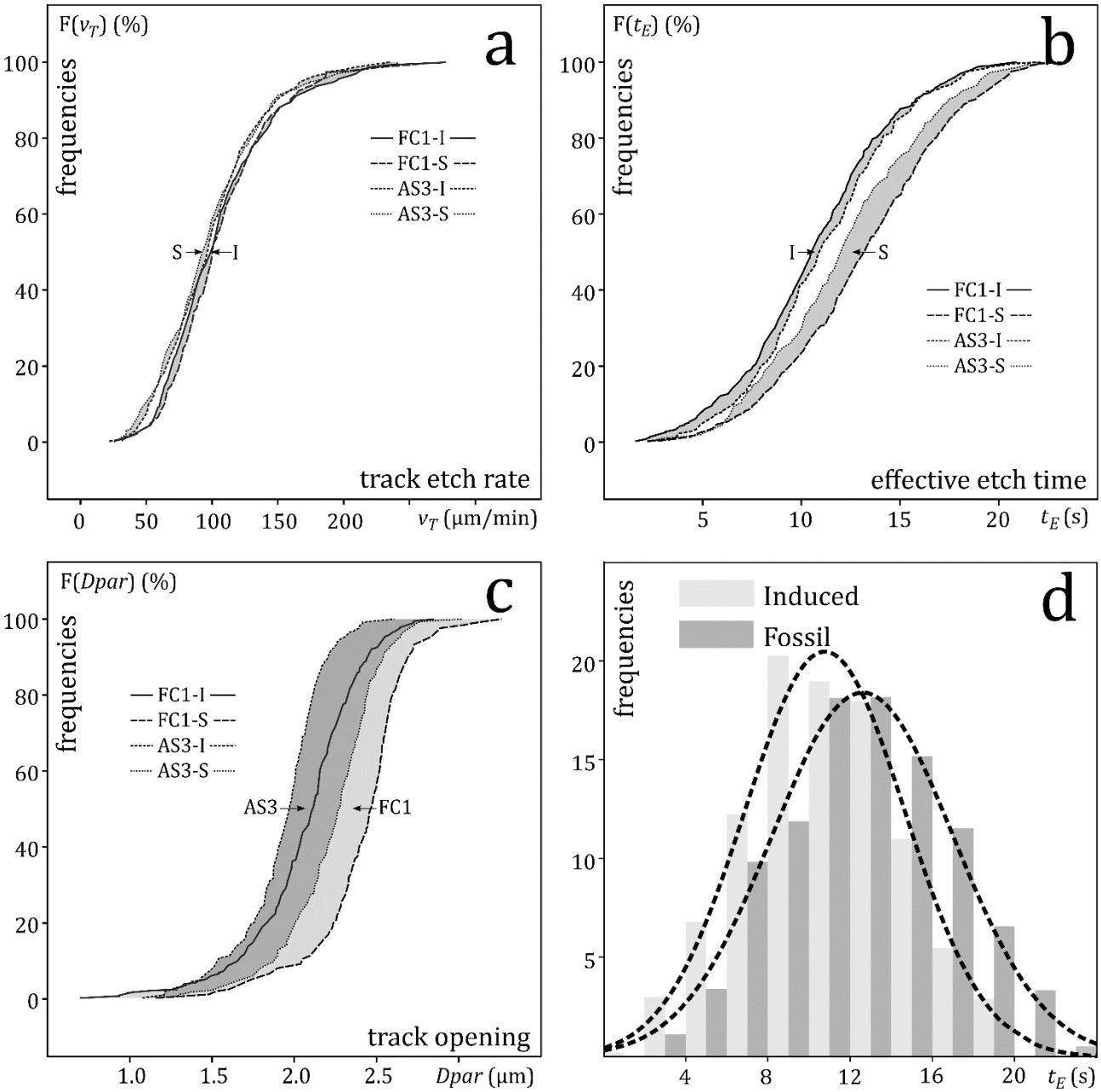

Figure 8. (a) Cumulative frequencies of the track etch rates of fossil (S) and induced (I) confined tracks in the FC-1 and AS-3 apatites **(b)** Cumulative frequencies of the effective etch times of fossil and induced tracks **(c)** cumulative frequencies of the sizes of the track surface intersections (*Dpar*) of fossil and induced tracks. (d) Histograms of the effective etch times of the combined fossil and induced tracks of FC-1 and AS-3.

The major difference between samples FC1 and AS3, and between the fossil and induced tracks in each, is between their *Dpar*-values (Table 4; Figure 8c). The fossil-track values are ~16% (AS3) and ~17% (FC1) greater than those of induced tracks. We propose that this is due to distributed radiation damage from α-disintegration of ^{238}U, ^{235}U, ^{232}Th, and ^{147}Sm, and from collateral recoils from ^{238}U-fission, accumulated over geological time. The resulting lattice damage increases the overall apatite etch rate, producing larger *Dpar*. Figure 9 shows the openings of fossil and induced tracks in FC1. The ageing of the fossil-track samples appears to have had a greater effect on the widths (*Dper*) than on the lengths (*Dpar*) of the track-surface intersections. This support the radiation damage idea: *Dpar* depends on the etch rates of fast etching faces while *Dper* depends on that of slow-etching prism faces flanking each track to either side (Jonckheere et al., 2020; 2022). This can account for the doubling of *Dper* while *Dpar* increases <20% (Figure 9b), as slow-etching faces are more susceptible to radiation damage than fast etching faces (Jonckheere et al., 2019; their Figure 4). Tamer and Ketcham (2020b), in contrast, found no difference between the *Dpar* of fossil and induced tracks in the Durango, Fish Canyon Tuff, and Tioga apatites. Depending on uncertain estimates of the U, Th-concentrations and damage accumulation ages, it is just possible that the FC1 apatite is, or once was, past the first damage percolation point, whereas the younger samples are, or were, not.

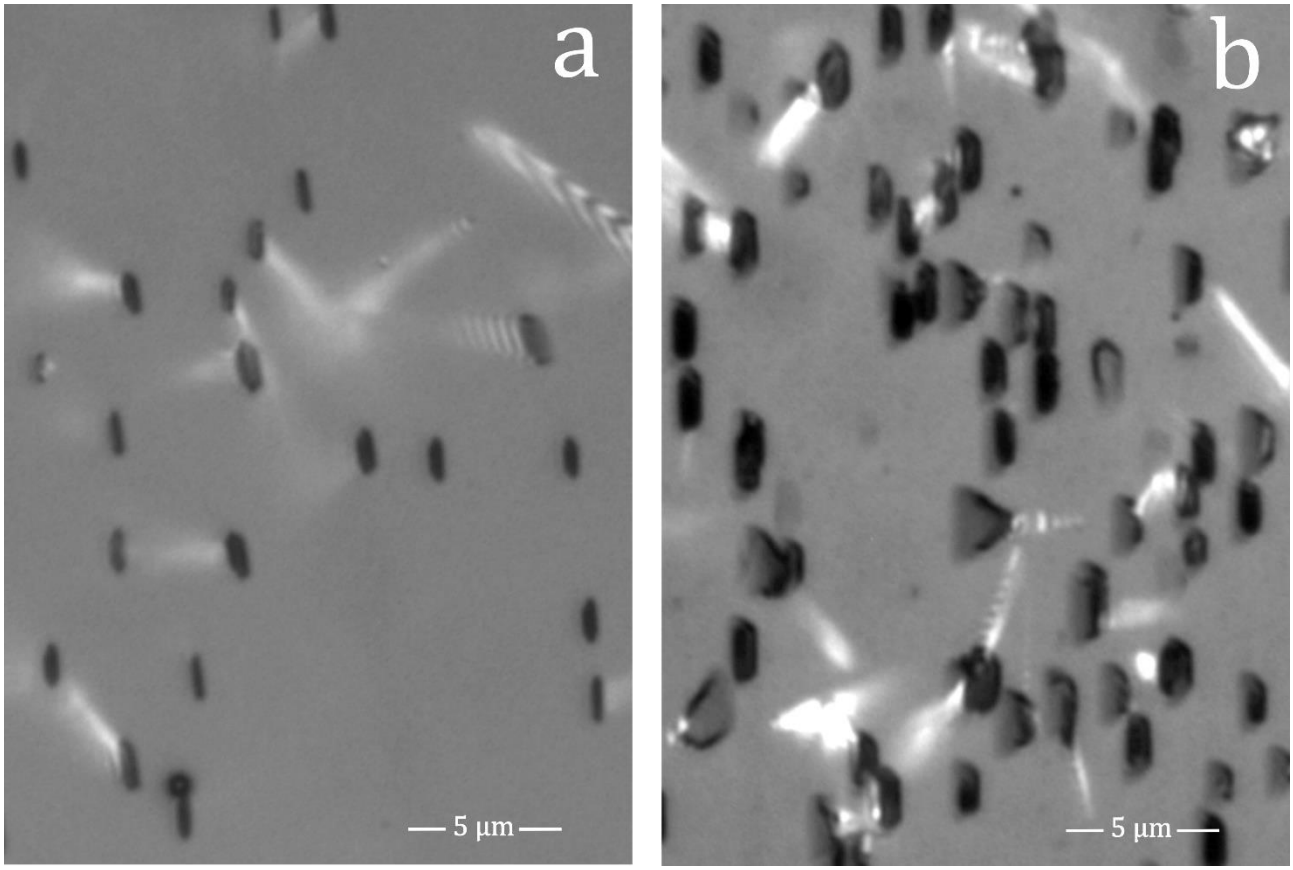

Figure 9. Reflected-light images of the openings of induced **(a)** and fossil **(b)** tracks in prism faces of the FC1 apatite (etched 20 s in 5.5 M HNO_3 at 21 °C).

Supplement Figure S15 plots the ***c***-axis-projected lengths (l_P) of individual confined tracks against their effective etch times (t_E), and Figure S16 against their track etch rates (v_T). The results for the induced tracks in FC1-I and AS3-I are in part similar to those for the unannealed Durango sample (21-2; Table 2). As in sample 21-2, the variation of v_T adds 0.1-0.2 µm to the lengths of the fastest etching tracks, compared to those of the slowest etching tracks. In contrast, the variation of t_E

causes a 0.6-µm length difference over the full t_E-range, compared to 0.1 µm for 21-2. The results for the fossil tracks in AS3-S are similar to those for the induced tracks in AS3-I (0.2 µm length difference due to v_T; 0.6 µm due to t_E), but those for the fossil tracks in FC1-S are not (0.7 µm length difference due to v_T; 0.2 µm due to t_E). On the whole, the v_T- and t_E-variation between tracks has little effect on the length distribution of a confined track population etched in a single 20 s step. However, as mentioned, the ordinary least squares regression underestimates the true slopes of the regression lines.

5. Synthesis

Our measurements and microscopic observations indicate that v_T is constant over most of the length of ion and fission tracks in apatite (constant core model; Tamer and Ketcham, 2020a). This suggests that there is a threshold damage above which v_T does not increase, e.g., an amorphous core raises v_T to a value that does not depend on the work expended to create it (i.e., the amorphous state is an end state). However, that is not within the scope of our investigation. On the other hand, reconciling straight-sided etched surface and confined tracks with something other than a constant v_T requires a different and more complex etch model than any proposed to date. We report 3588 of v_T-values, consistent with earlier results, based on measurements of the track widths and shapes. These are the only estimates in existence except for predetermined v_T-profiles fitted to 28 track lengths. Since the track length integrates the along-track v_T-variation over the full immersion time, it is improbable that the latter approach has more than the most indirect and tenuous bearing on v_T. It is therefore no surprise that the preferred linear model conflicts with the observed track shapes, in contrast with ours which is consistent with the straight sided confined track in Figure 4a, and surface tracks in Figure 4b. No conceivable other model does that. Our results also revealed that the etchant advances at a high but finite rate along pre-etched tracks. This implies that the summed immersion times of step-etch experiments are overestimates, and that step-etching broadens the effective-etch-time distribution (Jonckheere et al., 2024a; their Figure 6a). It also implies that successive etch steps cause v_T to be underestimated to an increasing extent (Jonckheere et al., 2024a; their Figure 5c). The low average v_T of fossil tracks in Durango apatite of Aslanian et al. (2021; ~75 µm·min^{-1}) is therefore not in conflict with the present results.

The distributions of host-track intersections (i_P), ***c***-axis angles (ϕ), and track-etch rates (v_T) are almost identical across all measurements. There is a noticeable offset between the average v_T of the Durango and Duluth samples, but this must not mean that it is of fundamental importance. The calculation of v_T requires v_R, which was measured for Durango (Aslanian et al., 2021) and some other apatites but not for FC1 and AS3, whose etch rates were estimated from their *Dpar*-values, relative to that of Durango (Trilsch et al., 2023; Fu et al., 2024). The difference between Durango and Duluth could be within the uncertainties, which could also account for the small difference between the fossil and induced tracks in FC1 and AS3. The near-identical i_P-, ϕ-, and v_T-distributions are difficult to explain, but suggest that the confined-track selection is dominated by a criterion that is more or less independent of the track densities or lengths. The confined-track width is such a criterion that is moreover little affected by annealing (Jonckheere, 2023).

In contrast to the track etch rate v_T, the apatite etch rate v_R shows marked variation. This is most obvious from the *Dpar*-values of the fossil and induced tracks in FC1 and AS3, but also from those of the annealed induced tracks in Durango apatite. In the case of the fossil tracks, the *Dper*/*Dpar*-ratio increases as well as *Dpar*. It is therefore probable that the *Dpar*-increases are related to lattice damage, from the natural background radiation in the fossil-track samples and from neutron irradiation in the induced-track samples. *Dper*/*Dpar-ratios* could offer a means of assessing damage densities in apatite if their effect can be separated from chemical effects on *Dpar*. On the other

hand, *Dpar*-variation implies a need for caution when using *Dpar* for estimating apatite annealing rates. The greater v_R of the Duluth samples with fossil tracks increases the rate of advance of the etchant along the slowest section of its course down the host track (v_T), across to the confined track (v_R; widening of the host track) and along the confined track to each tip (v_T). Confined tracks in fast etching apatites therefore have shorter access times and, in consequence, longer effective etch times.

6. Conclusion

Since the earliest fission track studies, all etch models have been based on two velocities: v_T, the rate of advance along the damaged track core, and v_R, the rate of retreat of the undamaged material. These velocities are more than conceptual: their values define the efficiencies of the track counts (Tagami and O'Sullivan, 2005) and thresholds for confined-track selection (Ketcham and Tamer, 2021; Jonckheere, 2023). They also provide the basis for explaining the shapes of etched tracks (Jonckheere et al., 2022). On its own, v_R is an important indicator of chemical composition and annealing kinetics (*Dpar*; Burtner et al., 1994). Actual measurements of v_T and v_R have however long been missing.

The reported measurements show that some long-standing assumptions concerning apatite and fission-track etching are not corroborated by the evidence. The track etch rate v_T is little dependent on the track forming process (dE/dx), and is little affected by either lab or geological annealing. In contrast, the apatite etch rate v_R, besides its dependence on composition, does seem to be somewhat affected by annealing and in some samples by ageing. This revised picture has practical implications for the interpretation of track etching, track selection, and the estimation of thermal histories.

Data availability

Data are available as Excel files Krypton.xlsx (section2), Durango.xlsx (section3), and Duluth.xlsx (section 4) in supplement.

Author contributions

Concept, funding and administration: RJ, TN; data curation, statistics, discussion and interpretation: RJ, FT, JL, PZ; manuscript text, figures and tables: RJ, FT, TN; replies to reviews and revision: RJ, TF.

Competing interests

The contact author declares that neither they nor their co-authors have any competing interests.

Acknowledgment

We thank the accelerator staff at the Heavy Ion Research Facility Lanzhou of the Institute of Modern Physics of the Chinese Academy of Sciences for their expert handling of the Kr-irradiation. We are indebted to Hideki Iwano for providing generous aliquots of the FC1 and AS3 Duluth apatites. The authors thank Richard Ketcham and an unnamed reviewer for their constructive comments.

Financial support

Funded by the German Science Foundation (Grant JO 358/6).

7. References

Aslanian C., Jonckheere R., Wauschkuhn B., Ratschbacher L. (2021) A quantitative description of fission-track etching in apatite. American Mineralogist 106, 518-526.

Aslanian C., Jonckheere R., Wauschkuhn B., Ratschbacher L. (2022) Short communication: Experimental factors affecting fission-track counts in apatite. Geochronology 4, 109-119.

Boyce J.W., Hodges K.V. (2005) U and Th zoning in Cerro de Mercado (Durango, Mexico) fluorapatite: insights regarding the impact of recoil redistribution of radiogenic 4He on (U–Th)/He thermochronology. Chemical Geology 219, 261–274.

Bobroff N. (1986) Position measurement with a resolution and noise-limited instrument. Review of Scientific Instruments 57, 1152-1157.

Burtner R.L., Nigrini A., Donelick R.A. (1994) Thermochronology of Lower Cretaceous source rocks in the Idaho-Wyoming thrust belt. American Association of Petroleum Geologist Bulletin 78, 1613-1636.

Carlson W.D., Donelick R.A, Ketcham R.A. (1999) Variability of apatite fission-track annealing kinetics: I. Experimental results. American Mineralogist 84, 1213-1223.

Cogné N., Gallagher K. (2021) Some comments on the effect of uranium zonation on fission track dating by LA-ICP-MS. Chemical Geology, 573, 120226.

Copeland C.R., Geist J., McGray C.D., Aksyuk V.A., Liddle J.A., Ilic B.R., Stavis S.M. (2018) Sub-nanometre localization accuracy in widefield optical microscopy. Light: Science & Applications 7:31, 1-15.

Donelick R.A., Ketcham R.A., Carlson W.D. (1999) Variability of apatite fission-track annealing kinetics: II. Crystallographic orientation effects. American Mineralogist 84, 1224-1234.

Dufour C., Toulemonde M. (2016). Models for the Description of Track Formation. In: W. Wesch and E. Wendler, eds., Ion Beam Modification of Solids, Springer Series in Surface Sciences, 61, 63-101.

Durrani S.A., Bull R.K. (1987) Solid state nuclear track detection. Principles, methods and applications. Pergamon Press, Oxford, pp. 304.

Enkelmann, E., Jonckheere, R., Ratschbacher, L., 2005a. Absolute measurements of the uranium concentration in thick samples using external fission-track detectors. Nuclear Instruments and Methods in Physics Research B 229, 489-498.

Enkelmann, E., Jonckheere, R., Wauschkuhn, B., 2005b. Independent fission-track ages (ϕ-ages) of proposed and accepted apatite age standards and a comparison of ϕ-, Z-, ζ- and ζ_0-ages: implications for method calibration. Chemical Geology 222, 232-248.

Fleischer R.L. & Price P.B. (1964) : Techniques for geological dating of minerals by chemical etching of fission fragment tracks. Geochimica et Cosmochimica Acta 28,1705-1714.

Fleischer R.L., Price P.B., Walker R.M. (1975) Nuclear tracks in solids. Principles and applications. University of California Press, Berkeley, pp. 604.

Fleischer R.L., Price P.B., Woods R.T. (1969) Nuclear-particle-track identification in inorganic solids. Physical Review 188, 563-568.

Foshag W.F. (1929) Mineralogy and geology of Cerro de Mercado, Durango, Mexico. Proceedings of the U.S. National Museum 74, 1-27 + 4 plates.

Fu Hongyang, Trilsch F., Jonckheere R., Ratschbacher L. (2024) Compositional effects on the etching of fossil confined fission tracks in apatite. American Mineralogist 109, 2026-2036.

Galbraith, R.F. (2002). Some remarks on fission-track observational biases and crystallographic orientation effects. American Mineralogist 87, 991-995.

Galbraith R.F., Laslett G.M., Green P.F., Duddy I.R. (1990) Apatite fission track analysis: geological thermal history analysis based on a three-dimensional random process of linear radiation damage. Philosophical Transactions of the Royal Society of London A332, 419-438.

Gleadow A.J.W. (1981) Fission track dating methods: what are the real alternatives ? Nuclear Tracks 5, 3-14.

Gross, R. (1918) On the theory of growth and dissolution processes of crystalline matter. Abhandlungen der mathematisch-physischen Klasse der königlichen Sächsischen Gesellschaft der Wissenschaften zu Leipzig 35, 137-202 (in German).

Härtel B., Jonckheere R., Krause J., Ratschbacher L. (2022) Spurious age-eU associations in thermochronology. Earth and Planetary Science Letters, 117870.

Härtel B., Matthews W.A., Enkelmann E. (2023) Duluth complex FC1 apatite and zircon: Reference materials for (U-Th)/He dating? Geostandards and Geoanalytical Research. doi: 10.1111/ggr.12492

Heimann R.B. (1975) Dissolution of crystals. Theory and practical application. Applied Mineralogy 8, Springer, pp. 270 (in German).

Heimann R.B. (1982) Principles of Chemical Etching - The art and science of etching crystals. Silicon Chemical Etching, 173–224. Springer Berlin, Heidelberg.

Hurford A.J., 2019. An historical perspective on fission-track thermochronology. In: M.G. Malusà and P.G. Fitzgerald, Eds., Fission-Track Thermochronology and its Application to Geology, Geography and Environment, 3-23.

Iwano H., Danhara T., Yuguchi T., Hirata T., Ogasawara M. (2019) Duluth Complex apatites: Age reference material for LAICP-MS-based fission-track dating. Terra Nova, 31, 247-256.

Jonckheere R. (2003) On the ratio of induced fission-track densities in a mineral and a co-irradiated muscovite external detector with reference to fission-track dating of minerals. Chemical Geology 200, 41-58.

Jonckheere R. (2023) On etching, selection and measurement of confined fission tracks in apatite. Geochronology Discussions [preprint].

Jonckheere R., Aslanian C., Fu Hongyang, Trilsch F. (2024a) Sampling confined fission tracks for constraining geological thermal histories. Minerals 14, 1-16.

Jonckheere R., Aslanian C., Wauschkuhn B., Ratschbacher L. (2022) Fission-track etching in apatite: A model and some implications. American Mineralogist 107, 1190-1200.

Jonckheere R., Aslanian C., Wauschkuhn B., Ratschbacher L. (2020) Some geometrical properties of fission-track-surface intersections in apatite. American Mineralogist 105, 1355-1364.

Jonckheere R., Härtel B., Iwano H. (2024b) Fission-track age calibration: Phi and Zeta, never the twain shall meet? Chemical Geology 648, 121898.

Jonckheere R., Mars M., Van den haute P., Rebetez M., Chambaudet A. (1993) The apatite from Durango, Mexico: analysis of a standard mineral for fission-track dating. Chemical Geology 103, 141-154 (in French).

Jonckheere R., Van den haute P. (1996) Observations on the geometry of etched fission tracks in apatite: implications for models of track revelation. American Mineralogist 81, 1476-1493.

Jonckheere R., Van den haute P., Ratschbacher L. (2015) Standardless fission-track dating of the Durango apatite age standard. Chemical Geology 417, 44-57.

Jonckheere R., Wauschkuhn B., Ratschbacher L. (2019) On growth and form of etched fission tracks in apatite: A kinetic approach. American Mineralogist 104, 569-579.

Ketcham R.A. (2003) Observations on the relationship between crystallographic orientation and biasing in apatite fission-track measurements. American Mineralogist 88, 817-829.

Ketcham R.A., Carter A., Hurford A.J. (2015) Inter-laboratory comparison of fission track confined length and etch figure measurements in apatite. American Mineralogist 100, 1452-1468.

Ketcham R.A., Tamer M.T. (2021) Confined fission-track revelation in apatite: how it works and why it matters. Geochronology 3, 433-464.

Laslett G.M., Gleadow A.J.W., Duddy I.R. (1984) The relationship between fission track length and track density in apatite. Nuclear Tracks 9, 29-38.

Li Weixing, Kluth P., Schauries D., Rodriguez M.D., Lang M., Zhang Fuxiang, Zdorovets M., Trautmann C., Ewing R.C. (2014) Effect of orientation on ion track formation in apatite and zircon. American Mineralogist 99, 1127-1132.

Li Weixing, Lang M., Gleadow A.J.W., Zdorovets M.V., Ewing R.C. (2012) Thermal annealing of unetched fission tracks in apatite. Earth and Planetary Science Letters 321-322, 121-127.

Li Weixing, Shen Yahui, Zhoua Yueqing, Zhai Pengfei, Nana Shuai, Liu Jie, Ewing R.C. (2023) Unexpectedly narrower track diameter at site of fission event. Earth and Planetary Science Letters 616, 118217.

McConnel D. (1973) Apatite. Its crystal chemistry, mineralogy, utilization and geologic and biologic occurrences. In: Frechette, V.D., Kirsch, H., Sand, L.B., Trojer, F. (Eds.), Applied Mineralogy 5. Springer Verlag, Wien 111 pp.

Nikezić D. (2000) Three-dimensional analytical determination of the track parameters. Radiation Measurements 32, 277-282.

Nikezić D., Yu K.N.(2003) Three-dimensional analytical determination of the track parameters: over-etched tracks. Radiation Measurements 37, 39-45.

Nikezić D., Yu K.N.(2004) Formation and growth of tracks in nuclear track materials. Materials Science and Engineering 46, 51-123.

Paretzke H.G., Benton E.V., Henke R.P. (1973) On particle track evolution in dielectric track detectors and charge identification through track radius measurement. Nuclear Instruments and Methods 108, 73-80.

Rivera A., Garcia G., Olivares J., Crespillo M.L. and Agulló-López F. (2011) Elastic (stress–strain) halo associated with ion-induced nano-tracks in lithium niobate: role of crystal anisotropy. Journal of Physics D: Applied Physics 44, 475301 (11pp).

Rymzhanov R.A., Gorbunov S.A., Medvedev N., Volkov A.E. (2019) Damage along swift heavy ion trajectory. Nuclear Instruments and Methods in Physics Research B 440, 25-35.

Schauries D. (2018) Ion tracks in apatite and quartz and their behaviour with temperature and pressure. Ph.D. Thesis, Australian National University. Springer Theses ISSN 2190-5053,pp. 166.

Somogyi G., Szalay S.A. (1973) Track diameter kinetics in dielectric track detectors. Nuclear Instruments and Methods 109, 211-232.

Tagami T., O'Sullivan P.B. (2005) Fundamentals of fission-track thermochronology. Reviews in Mineralogy and Geochemistry 58, 19-47.

Tamer M.T., Ketcham R.A. (2020a) The along-track etching structure of fission tracks in apatite: Observations and implications. Chemical Geology 553, 119809.

Tamer M.T., Ketcham R.A. (2020b) Is low-temperature fission-track annealing in apatite a thermally controlled process? Geochemistry, Geophysics, Geosystems 21, e2019GC008877.

Trilsch F., Fu Hongyang, Jonckheere R., Ratschbacher L. (2023) Effective etch times of fossil fission tracks in geological apatite samples and impact on temperature-time modelling. Lithosphere (Special 14), lithosphere_2023_339.

Young E.J., Myers A.T., Munson E.L., Conklin N.M. (1969) Mineralogy and geochemistry of fluorapatite from Cerro de Mercado, Durango, Mexico. U.S. Geological Survey Professional Paper 650, pp. 84-93.